Simulation and experimental study of asymmetric split and recombine micromixer with D-shaped sub-channels

Xiuhua He[1] ✉, *Tian Xia*[1], *Linfeng Gao*[1], *Zhidan Deng*[2], *Benjamin B. Uzoejinwa*[1,3]

[1]*School of Energy and Power Engineering, Jiangsu University, Zhenjiang, Jiangsu, People's Republic of China*
[2]*Faculty of Science, Jiangsu University, Zhenjiang, Jiangsu, People's Republic of China*
[3]*Department of Agricultural and Bioresources Engineering, University of Nigeria, Nsukka, Nigeria*
✉ *E-mail: xiuhua.he@ujs.edu.cn*

Published in Micro & Nano Letters; Received on 24th May 2018; Revised on 10th November 2018; Accepted on 22nd November 2018

An effective passive micromixer based on the principles of asymmetric split and recombine has been designed, developed, and investigated to enhance the mixing performance of the micromixer in a microfluidic system. The effects of geometrical parameters and the number of mixing units on mixing performance were studied at different Reynolds (Re) number (ranging from 1 to 80) via CFD software ANSYS CFX. The results revealed that the preferable number of mixing units is 6, and the optimal direction of reducer is opposite to the main channel flow; the D-shaped mixing channel forces the mixed fluid to produce the extended vortex and Dean vortices simultaneously which caused a strong collision at the confluence of fluids, thus leading to the superposition and enhancement of the vortex system; when Re number is 80 and the width ratio of mixing channel $W2/W3 = 1$, the mixing efficiency of micromixer can exceed 95%.

1. Introduction: Micromixer is one of the most crucial components of the microfluidic system, which draws increasing attention and obtains wide applications with the flourishing development of microelectromechanical systems. For two decades, domestic and foreign scholars have designed various micromixers to meet the requirement of reagent homogenisation in the biochemical field [1–3]. The rapid mixing of different fluids is a prerequisite for a complete reaction in the biochemical process. Thus, it is very important to achieve rapid mixing of different fluids in a microscale [4, 5]. The micromixer has a high specific surface area and special flow characteristics, which can accelerate the reaction speed of the mixed fluid, and consequently, it has a broad application prospect [6–8].

Micromixer can be divided into active and passive types based on the availability of additional power sources [9–11]. The passive micromixer becomes the main research target because it has no additional power source which means simpler structure and easier integration compared to the active counterpart, and furthermore, the mixing process in it does not change the physical and chemical properties of the samples. The design of different structural types on microchannel and the change of diverse flow conditions on the mixed fluid are the primary research contents that have gained a huge interest in the recent years [10–15]. He *et al.* [16] designed a passive micromixer based on the logarithmic helix that caused chaotic convection of the mixed fluid through a curved flow channel. Ansari and Kim [17] designed an unbalanced split and recombine micromixers with circular and rhombic sub-channels which enhanced the chaotic convection intensity and improved the mixing efficiency by recombining the separated fluids. Chen and Shen [18] also designed a micromixer with the E-shaped structure using the principle of split and recombine, so that the fluids can mix quickly in the three-dimensional channels. However, the complex structure makes the manufacturing process more difficult.

This Letter presents a novel D-shaped split and a recombine micromixer. The micromixer makes the mixed fluid to produce convection and vortices by changing the geometric structure of the flow channels. The flow characteristics and the mixing efficiency of the mixed fluid were investigated at Reynolds (Re) number ranging from 1 to 80 by numerical simulation. Meanwhile, the influence of different structural parameters on mixing efficiency was analysed, and the simulation results were also verified through experiments.

2. Numerical simulation: The scale of this newly designed micromixer ranges from dozens to hundreds of microns, which is much larger than the molecular mean free path so that the fluid flowing in the microchannel can be regarded as an incompressible viscous fluid. The continuity equation, the Navier–Stokes equation for an incompressible fluid and the convection–diffusion equation can be reduced to (1)–(3) with no-slip boundary condition:

$$\nabla \cdot (\boldsymbol{u}) = 0 \tag{1}$$

$$\boldsymbol{u} \cdot \nabla \boldsymbol{u} = -\frac{1}{\rho}\nabla P + \nu \nabla^2 \boldsymbol{u} \tag{2}$$

$$D\nabla^2 C = \boldsymbol{u} \cdot \nabla C \tag{3}$$

where $\boldsymbol{u}$, ρ, P, D, ν, and C represent the fluid velocity vector, fluid density, pressure, diffusion coefficient, kinematic viscosity and fluid concentration, respectively.

The adiabatic and steady mixing process of the incompressible fluids in the micromixer was simulated by ANSYS CFX. The continuity equation, the Navier–Stokes equation, and the convection–diffusion equation were used as control equations during the numerical simulation. There is no energy equation here, because no chemical reaction occurred in the mixing process. The SIMPLEC algorithm was utilised for the pressure-velocity coupling. The inlet is set as the speed boundary condition, while the outlet is set as the pressure boundary condition, and the relative static pressure is set to zero.

The mass fraction of the two fluids to be mixed is set to 1 and 0, respectively during the numerical simulation. Keeping the volume flow rate of the two fluids to be mixed consistently simplifies the calculation. The Re number in this study ranges from 1 to 80, which means the flow condition changes from laminar flow to turbulent flow, thus covering three different flow states: stratified flow, vortex flow, and engulfment flow. Re number is calculated by using the physical parameters of the mixed fluid and the hydraulic diameter of micromixer inlet, and the formula is

$$\mathrm{Re} = \rho v d/\mu \tag{4}$$

where ρ is the fluid density, v is the fluid velocity at the inlet, d is the hydraulic diameter at the inlet, and μ is the hydrodynamic viscosity.

The mixing efficiency is the key indicator of micromixer performance, which will directly affect the quality and quantity of various reactions. In order to quantitatively evaluate the degree of mixing in the micromixer, the mixing efficiency was defined as M, and the calculation method is as shown in (5) [19, 20]

$$M = \left(1 - \frac{\int_0^{\omega} |C - C_{\infty}| \, \mathrm{d}x}{\int_0^{\omega} |C_0 - C_{\infty}| \, \mathrm{d}x}\right) \times 100\% \tag{5}$$

where C is the fluid mass fraction at the outlet, C_{∞} is the fluid mass fraction when the mixing is complete (here $C_{\infty} = 0.5$ means that the mass fraction of two fluids is the same in each region after the mixing), C_0 is the fluid mass fraction before the start of mixing, and ω is the width of outlet. According to the formula, the mixing efficiency M is in the range of 0–1, and larger the value of M, the higher the mixing efficiency. When $M = 1$ it means that the two media have been completely mixed, and when $M = 0$ it means that the two media are not mixed at all.

In this Letter, the software Gambit was used to mesh the micromixer geometric model, and the grid type is an unstructured hexahedral mesh. In order to improve the calculation speed for ensuring the reliability of the results, the grid encryption was taken only for the key areas (such as the tapered pipe, mixing area, outlet etc.), and the block coupling method was used to weaken the influence of diffusion value in the simulation. When the number of grids is 3.96×10^5, 7.93×10^5, and 1.226×10^6, the simulation results of the mixing efficiency were compared with the results when the number of grids is 2.205×10^6. The maximum errors are 8.12, 1.22 and 0.047%. Thus, the total number of grids can be set as 1.226×10^6 for the purpose of improving the calculation speed.

Fig. 1*a* shows the schematic diagram of the micomixer with D-shaped sub-channels. The main parameters are as follows: entrance width $W = 200$ μm, D-shaped channel length $L_1 = 1200$ μm, exit length $L_2 = 1800$ μm, exit width $W_4 = 150$ μm. The total length of the micromixer is 10,200 μm. Fig. 1*b* is the enlarged view of the D-shaped unit in which the radius of the semicircular split wall is the same as W, the width of straight sub-channel W_3 in the D-shaped unit is 150 μm, and the width of bent sub-channel $W_2 = 150$ μm. The radius R_0 of the outer wall of bent sub-channel is 600 μm, the inlet width of the tapered pipe is the same as W_2, and the width W_5 of the outlet is 60 μm.

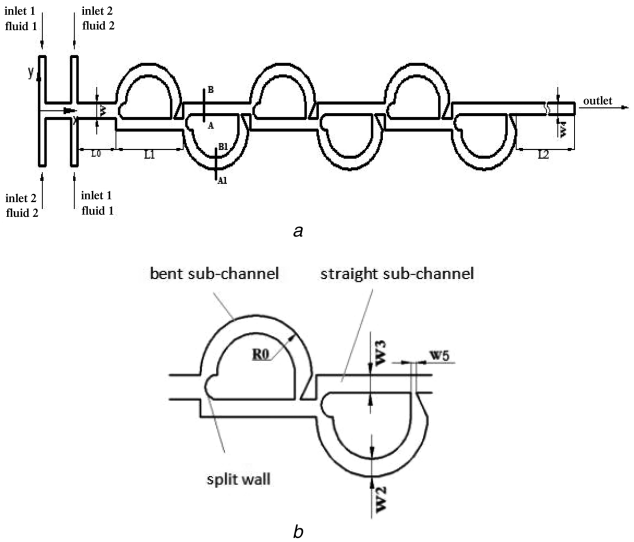

Fig. 1 *Micromixer design*
a Schematic diagram of the micromixer
b Enlarged view of mixing unit

3. Experiment procedures: As shown in Fig. 2, the chip of the micromixer was processed to verify the reliability and accuracy of the numerical simulation and observe the mixing performance of the micromixer in experiments. The chip has a two-layered structure, the material of the micromixer substrate is polydimethylsiloxane, and the plate of micromixer is made of Pyrex glass which has high hardness. A molding method is employed to produce the micromixer substrate. Finally, the method of static bonding was taken to achieve the chip.

To investigate the mixing performance of the micromixer with the D-shaped sub-channels, two reagents were injected into the inlets by a syringe pump (Longer LSP02-1B). One reagent with deionised water and another with deionised water that contained a few drops of black ink. The flow state in the flow channel was observed through an inverted microscope (Nikon ECLIPSE Ti-s). A CCD camera (Nikon DIGITAL SIGHT DS-Ri1) was used to shoot the flow state diagrams and import these diagrams to a computer for comparison. Eventually, the mixed solution was processed with a greyscale value. Then the corresponding mixing efficiency values were calculated and compared with the simulated values. As shown in Fig. 3, the simulation efficiency at different Re numbers is very close to the experimental value, which confirmed the validity of the numerical simulation used in this Letter.

4. Results and discussion: The influence of related structural parameters on the internal flow field and the mixing efficiency of the D-shaped split and recombine micromixer were revealed via the comparison between the simulation and experiment. Finally, the asymmetric D-shaped split and the recombine micromixer with optimum mixing performance were developed.

The individual structural type of D-shaped micromixer can change the mixing condition of the mixed fluid and eventually affects the mixing efficiency. The mixing distance of the micromixer possesses evident effects on the mixing efficiency, and

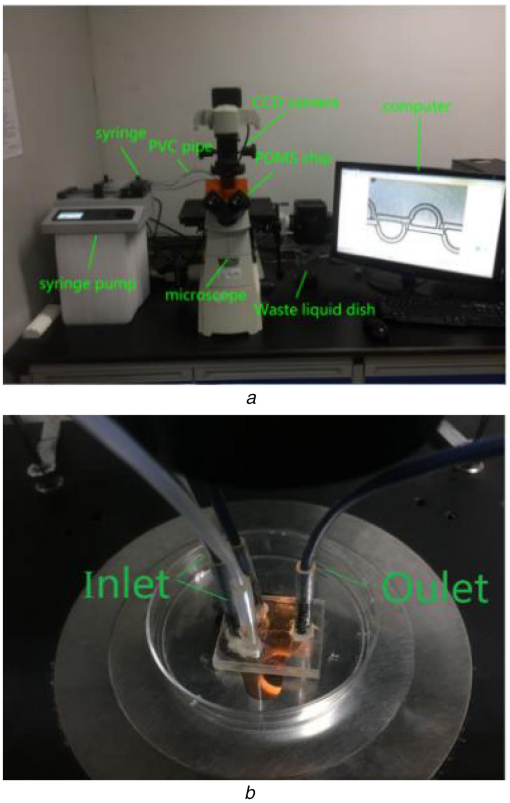

Fig. 2 *Micromixer chip processing*
a Picture of the experimental bench
b Enlarged view of working area

doi: 10.1049/mnl.2018.5219

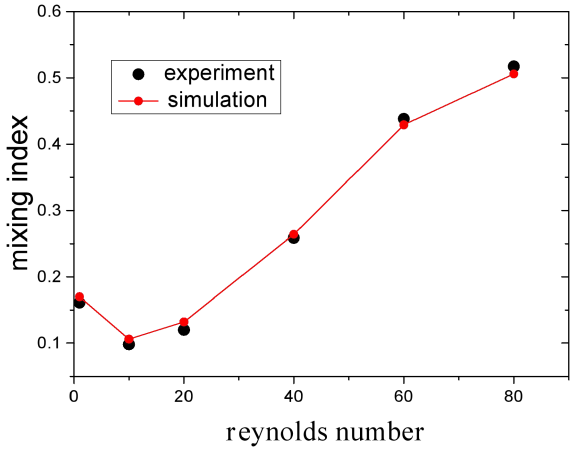

Fig. 3 *Comparison between the mixing efficiency M of the experiment and numerical simulation*

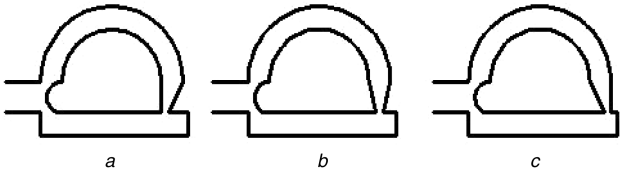

Fig. 4 *Different deflections of the reducer in bent sub-channel*

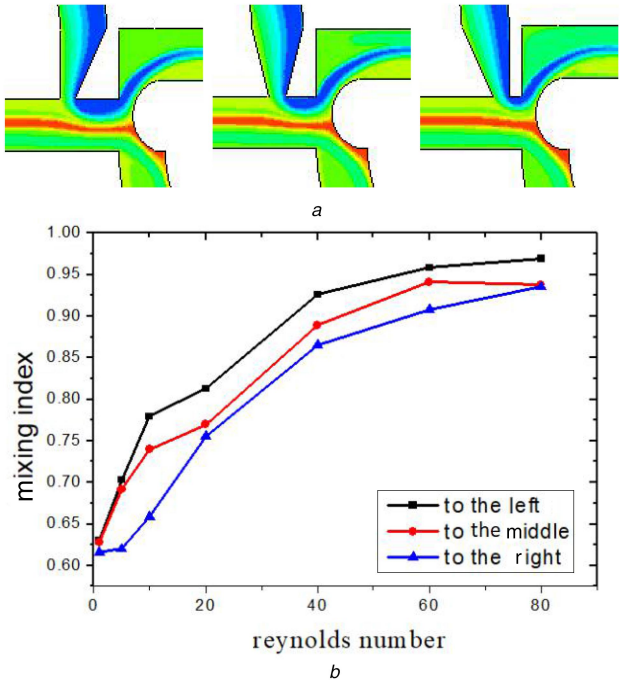

Fig. 5 *The effect of the reducer with different directions on the mixing performance of the micromixer*
a Flow patterns of three reducers (Re = 40)
b Effect of the reducer direction on mixing efficiency

meanwhile the reducer in the bent sub-channel, which has a great acceleration on the mixed fluid, also directly impacts the mixing efficiency. The direction of the reducer and the number of mixing units in the D-shaped micromixer, therefore, were further studied and analysed.

The direction of the reducer alters the flow direction of the mixed fluid in the bent sub-channel, which directly affects the collision severity of the mixed fluid between the bent sub-channel and the straight sub-channel, as a result, the mixing efficiency of the micromixer is influenced. Fig. 4 shows the three different deflections of the reducer, and Fig. 5 shows the effect of the reducer with different directions on the mixing performance of the micromixer. Fig. 5*a* shows the internal flow conditions of different reducers at Re = 40. When the mixed fluid in the bent sub-channel passes through the reducer (a) and generates a jet flow against the mixing flow direction leading to a severe collision between the two mixed fluids, the mixing efficiency increases due to the larger contact area and the stronger turbulence intensity. Fig. 5*b* indicates that the reducer (a) has the highest mixing efficiency, while the reducer (b) has the lowest.

Generally, a longer mixing channel means longer retention time and higher mixing efficiency for most mixers. However, the growing mixing time is not applicable in some cases that required rapid mixing. Hence, it is important to find a balance, and a better way is to try to shorten the total channel length with the premise of mixing efficiency. In order to select a favourable number of mixing units, different mixing unit numbers (4–7) of the micromixer are simulated and compared under different Re. It can be seen from Fig. 6 that the mixing efficiency rises with the increase of mixing unit number and mixing distance. As the number of D-shaped mixing units increases from 4 to 6, the mixing efficiency keeps an evident improvement of 10%. This is because the mixing between media does not reach saturation yet, and therefore the mixing efficiency rises significantly with the increase of mixing unit number and mixing distance. When the mixing unit number is 7, the mixing efficiency has only 1–3% deviation from the condition when that is 6, which indicates that the mixed fluid at the

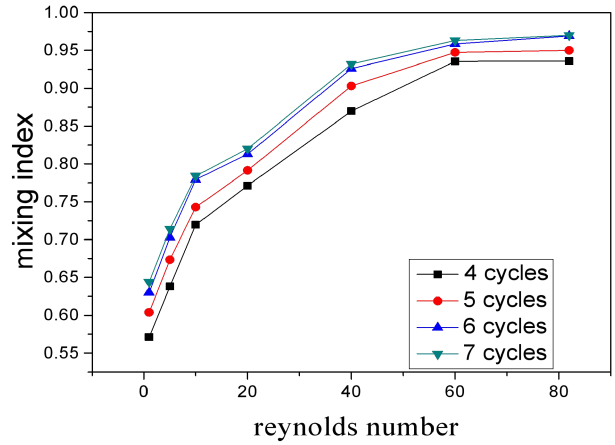

Fig. 6 *Effect of mixing unit numbers on the mixing efficiency under different Re*

outlet is close to saturation. So the effect of mixing distance on mixing efficiency is no longer obvious. Thus, the preferable number of mixing units here is 6.

According to the simulation on this novel passive micromixer, the D-shaped flow channel structure has a significant improvement on the mixing performance. As shown in Fig. 1, the mixed fluid in the main channel evenly flows into the straight sub-channel and the bent sub-channel through a semicircular split wall. Due to the sudden expansion at the connection between the straight sub-channel and semicircular split wall, the mixed fluid forms an extended vortex system at the entrance of the D-shaped channel, which disturbs the fluid flow in the microchannel and increases the contact area between the two fluids, thereby enhancing the mixing performance. The converging structure of the bent sub-channel improves the fluid velocity in it, and intensifies the collision between the mixed fluid at the junction of bent and straight

sub-channels, consequently increasing the disturbance. When the fluid passes through the bent sub-channel, a Dean vortex is formed at the cross-section perpendicular to the flow direction and a symmetric reverse vortex is formed in this section, because of the centrifugal force that the mixed fluid is subjected to. In the interaction of the semicircular split wall and straight sub-channel, the mixed fluid flowing into the straight sub-channel is also subjected to a large force perpendicular to the flow direction and forms a significant secondary flow, which accelerates the horizontal mass transfer flow of the mixed fluid.

Fig. 7 shows the streamlines of the cross-sections perpendicular to the flow direction (A–B and A1–B1, see in Fig. 1) at Re = 5, 40, and 80. It can be seen that when Re = 5, the A–B section has already emerged as an obvious reverse vortex. This is because the structure composed of the semicircular split wall and the D-shaped channel has a choking effect before the mixed fluid flows into the straight sub-channel, which gives a certain acceleration on the mixed fluid and exerts a large lateral force when it collides with the outer wall of the straight sub-channel. When the mixed fluid has lower velocity at the bent sub-channel, then there is no secondary flow observed at A1–B1 section. When Re = 40, the core velocity increases as the Re increases, but the velocity of the mixed fluid at the boundary is still low. Due to the effect of centrifugal force and shear stress generated in the D-shaped channel, the flow layer at the boundary produces significant deflection and flows to the inner side of the channel. Secondary flow is also emerged at A1–B1 section, while the secondary flow at the A–B section is enhanced. When Re = 80, the secondary flow at the A–B section becomes more intense, and two pairs of reverse vortices are formed. Meanwhile, there is a more complete secondary flow that emerged at the A1–B1 section.

Fig. 8 is the comparison between the concentration fields of the D-shaped mixing units and that of the experiment at different Re number. Due to the sudden expansion at the connection between the semicircular split wall and the D-shaped channel, the mixed flow forms an extended vortex in the D-shaped channel. When it passes through the reducer, the mixed fluid with high velocity in bent sub-channel has a violent collision with the mixed fluid in the straight sub-channel, disturbing the mixed fluid and thus changing the mixing condition in the straight sub-channel. By comparing the experimental results with the mixing unit at the same location, it was found that the simulated flow regime was maintained relatively consistent. When Re = 5, because of the low velocity, the two reagents in the mixing channel do not have an effective mixing, such that there is only a slender streamline of black reagent, and meanwhile the collision between the mixed

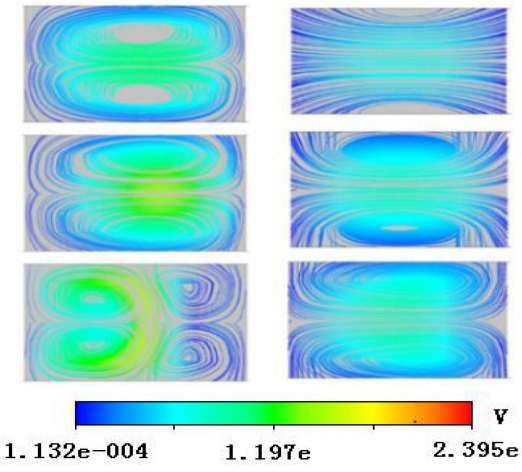

Fig. 7 *Streamlines of A–B (left) and A1–B1 (right) cross sections at different Re (Re = 5, 40, 80)*

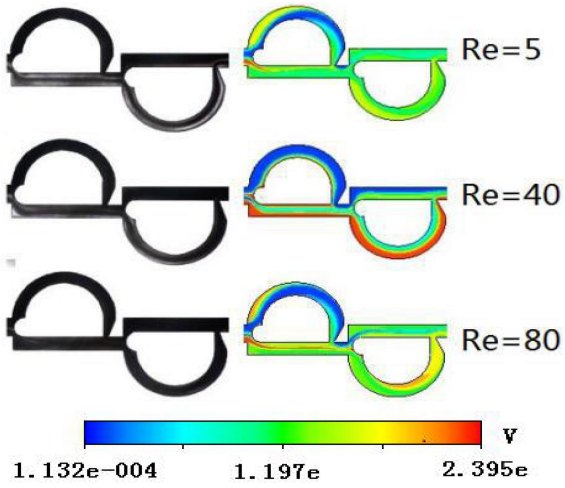

Fig. 8 *Comparison between concentration field of the D-shaped mixing unit and that from the experiment at different Re*

fluid of the sub-channel is not severe. When Re = 40, with the increase of the mixed fluid velocity and the influence of the asymmetric channel structure, the extended vortex system has gradually formed in the mixing channel, and the mixing activity in the straight sub-channel is more obvious. When Re = 80, with the collision between the mixed fluid becoming more intense, the mixing performance in the sub-channel is more apparent, and the mixed fluid's colour in the sub-channel becomes deeper.

As shown in Fig. 8, when Re = 5, due to the low velocity of the mixed fluid, no complete vortex system is formed in the D-shaped channel, and hence the disturbance is small, leading to low mixing degree. When Re = 40, many vortices have been formed basically in the D-shaped channel and mixing mainly depends on convection between the molecules, causing disturbance and larger contact area. Consequently, the mixing performance is better, and the mixing efficiency can reach about 93%. Fig. 9 is the concentration variation curve of the inlet and outlet of micromixer main channel in the axial direction (i.e. *y*-direction) at different Re number. Fig. 9*a* indicates that the mixing concentration at the inlet of the main channel is in a sinusoidal shape, due to the four entrances mode. It is because of the alternate mixing of the two mixed fluids, forming two layers of the contact surface, increasing the local disturbance of the two mixed fluids before entering the D-shaped mixing channel, and generating the trend of mixing flow. It can be seen by comparing Figs. 9*a* and *b* that the two mixed fluids formed a favourable mixing in their contact area at Re = 5, while the mixing has been basically completed at Re = 40.

According to the widths of the two sub-channels in the designed D-shaped channel, the width ratio C between bent sub-channel and straight sub-channel has been defined as $C = W2/W3$ (where the width of the straight sub-channel $W3$ remains the same), and the effect of C on the fluid mixing efficiency is studied by numerical simulation. Fig. 10 shows the mixing efficiency of the micromixer with the Re ($1 < \mathrm{Re} \leq 80$), which changes at different width ratios. It can be seen from the figure that when Re < 40, the mixing efficiency was increased rapidly and has not been affected by the small Re number and low velocity. It is because the four entrances structure accelerates the disturbance between the mixed fluids, and contributes to the formation of molecular convection disturbance and multi-directional vortices. However, the optimum mixing efficiency changes alternately with the increase of Re number at different width ratios. When Re<30, the micromixer reaches the optimum mixing efficiency at sub-channel width ratio $C = 1.2$, because the mixed fluid velocity is low at small Re, and no complete secondary flow is formed in the three D-shaped mixing units. When $C > 1$, due to the large bent sub-channel width of the

doi: 10.1049/mnl.2018.5219

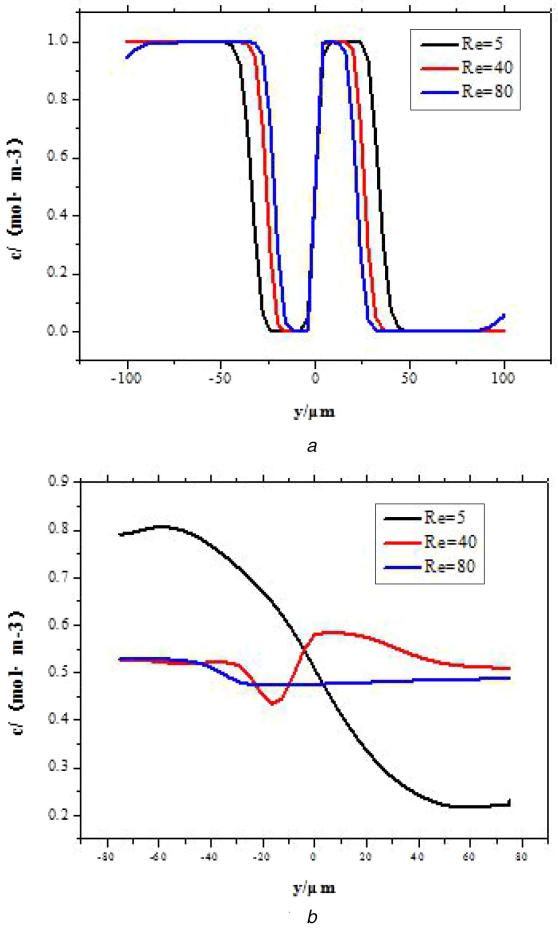

Fig. 9 *Mass fraction at*
a Inlet of micromixer
b Outlet of micromixer

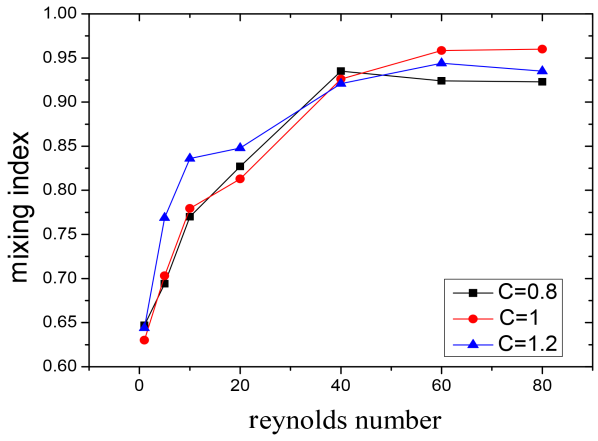

Fig. 10 *Effect of width ratio C on the mixing efficiency under different Re*

D-shaped mixing unit and the mass flow of the mixed fluid, the turbulent convection produced by the collision between the mixed fluids in bent sub-channel and straight sub-channel is stronger and the contact area is larger, leading to the higher mixing efficiency. When 30<Re≤40, there is a very little difference among these three micromixers. When Re ≥ 40, as the mixed fluid velocity increases continuously, a complete secondary flow is formed in both the bent sub-channel and the straight sub-channel. The mixing efficiency of $C = 1$ is the highest since its secondary flow is the most obvious.

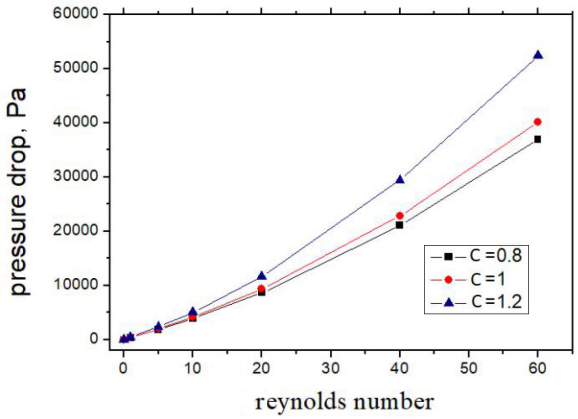

Fig. 11 *Effect of width ratio C on the pressure drop under different Re*

Fig. 11 shows the effect of the width ratio C on the pressure drop of the micromixer. It can be seen that the pressure drop increases with the increase of Re. The pressure drop varies little at the same Re when the width ratio $C = 0.8$ or 1, while it increases by a large margin when $C = 1.2$. It is because the mixed fluid flowing into the bent sub-channel increases as the width increases, but the width of the reducer outlet is very small, which brings a large loss to the mixed fluid in bent sub-channel, and as a result, the pressure drop of the whole asymmetric D-shaped split and recombine micromixer increases.

5. Conclusion: In this Letter, the influence of the reducer direction, the mixing unit numbers, the mixing channel width ratio on the mixing efficiency of the asymmetric D-shaped split and recombine micromixer have been investigated through numerical simulation, and the simulation method was validated through the experiment. The main conclusions are as follows:

(i) The double T-shaped inlet channel effectively increases the contact area of the mixed fluid. By using the principles of split and recombine, the mixed fluid is separated and remerged, and the collision at the merging causes a severe disturbance, which largely improved the mixing performance of the micromixer.

(ii) The simulation results showed that the optimum mixing efficiency can reach about 96% when the reducer direction is left, the number of mixing units is 6 and width ratio $C = 1$, comprehensively considering both the mixing efficiency and pressure drop.

(iii) The individual structure of the D-shaped split and recombine micromixer generates an enhanced Dean vortices in the vertical plane. The micromixer begins to form the convection disturbance of many vortex pairs at $Re = 5$, which significantly enhanced the mixing efficiency.

For future work, more entrance modes (e.g. unbalanced inlet structures, different width ratios of the inlet, etc.) on the mixing performance will be considered. Due to the limitation of equipment, the internal flow field of mixed fluid in the microchannel was not obtained here from the experiment. It is possible to employ microparticle image velocimetry (PIV) to get detailed information on the internal flow field for further research.

6. Acknowledgments: This work was supported by the National Natural Science Foundation of China (grant no. 51276082), and Departments of Education and Finance, Jiangsu Province of

PR China (A Project Funded by the Priority Academic Program Development of Jiangsu Higher Education Institutions, PAPD) (grant no. SUZHENGBANFA (2014) no. 37).

7 References

[1] Nguyen N.T., Wu Z.: 'Micromixers – a review', *J. Micromech. Microeng.*, 2005, **15**, pp. R1–R16

[2] Tsai R.T., Wu C.Y.: 'An efficient micromixer based on multidirectional vortices due to baffles and channel curvature', *Biomicrofluidics*, 2011, **5**, p. 14103

[3] Oosterbroek R.E., Berg A.J.V.D.: 'Lab-on-a-chip: miniaturized system for (bio) chemical analysis and synthesis' (Elsevier B V., Amsterdam, 2003)

[4] Stroock A.D., Dertinger S.K., Ajdari A., *ET AL.*: 'Chaotic mixer for microchannels', *Science*, 2002, **295**, pp. 647–651

[5] Erickson D.: 'Towards numerical prototyping of labs-on-chip: modeling for integrated microfluidic devices', *Microfluid. Nanofluid.*, 2005, **1**, pp. 301–318

[6] Ehrfeld W., Hessel V., Haverkamp V.: 'Microreactors' (Wiley-VCH Verlag GmbH & Co., Weinheim, 2000)

[7] Burke B.J., Regnier F.E.: 'Stopped-flow enzyme assays on a chip using a microfabricated mixer', *Anal. Chem.*, 2003, **75**, pp. 1786–1791

[8] Zhang X.T., Xu W., He X.H.: 'Characteristics of valveless piezoelectric micropump based on logarithmic spiral composite tube', *J. Drain. Irrig. Mach. Eng.*, 2017, **35**, pp. 119–132

[9] Hessel V., Lowe H., Schonfeld F.: 'Micromixers-a review on passive and active mixing principles', *Chem. Eng. Sci.*, 2005, **60**, pp. 2479–2501

[10] Capretto L., Cheng W., Hill M., *ET AL.*: 'Micromixing within microfluidic devices', *Top. Curr. Chem.*, 2011, **304**, pp. 27–68

[11] Kumar V., Paraschivoiu M., Nigam K.D.P.: 'Single-phase fluid flow and mixing in microchannels', *Chem. Eng. Sci.*, 2011, **66**, pp. 1329–1373

[12] Himstedt H.H., Yang Q., Dasi L.P., *ET AL.*: 'Magnetically activated micromixers for separation membranes', *Langmuir*, 2011, **27**, pp. 5574–5581

[13] Oddy M.H., Santiago J.G., Mikkelsen J.C.: 'Electrokinetic instability micromixing', *Anal. Chem.*, 2001, **73**, pp. 5822–5832

[14] Lee C.Y., Lee G.B., Fu L.M., *ET AL.*: 'Electrokinetically driven active micro-mixers utilizing zeta potential variation induced by field effect', *J. Micromech. Microeng.*, 2004, **14**, pp. 1390–1398

[15] Bhagat A.A.S., Peterson E.T.K., Papautsky I.: 'A passive planar micromixer with obstructions for mixing at low Reynolds numbers', *J. Micromech. Microeng.*, 2007, **17**, pp. 1017–1024

[16] He X.H., Wei D.D., Deng Z.D., *ET AL.*: 'Mixing performance of a novel passive micromixer with logarithmic spiral channel', *J. Drain. Irrig. Mach. Eng.*, 2014, **32**, pp. 968–972

[17] Ansari M.A., Kim K.Y.: 'Mixing performance of unbalanced split and recombine micomixers with circular and rhombic sub-channels', *Chem. Eng. J.*, 2010, **162**, pp. 760–767

[18] Chen X.Y., Shen J.N.: 'Numerical analysis of mixing behaviors of two types of E-shape micromixers', *Int. J. Heat Mass Transf.*, 2016, **106**, pp. 593–600

[19] Hossain S., Husain A., Kim K.Y.: 'Shape optimization of a micromixer with staggered-herringbone grooves patterned on opposite walls', *Chem. Eng. J.*, 2010, **162**, pp. 730–737

[20] Tran-Minh N., Karlsen F., Tao D., *ET AL.*: 'A simple and low cost micromixer for laminar blood mixing: design, optimization, and analysis. Biomedical informatics and technology', vol. 404 (Springer, Berlin, 2014), pp. 91–104

doi: 10.1049/mnl.2018.5219